Natural linear dichroism in pyrite (FeS_2): experiments and calculations

Delphine Cabaret,[a]* Christian Brouder,[a] Marie-Anne Arrio,[a] Philippe Sainctavit,[a] Yves Joly,[b] Andrei Rogalev[c] and José Goulon[c]

[a]LMCP, UMR7590, case 115, 4 place Jussieu, 75252 Paris cedex 05 France, [b]Laboratoire de cristallographie, CNRS, B.P. 166, 38042 Grenoble cedex 9 France, and [c]ESRF, B.P. 220, 38043 Grenoble cedex France. E-mail: cabaret@lmcp.jussieu.fr

Electric quadrupole transitions are revealed through the angular dependence of X-ray absorption spectra in a cubic crytal. Data collection was achieved at the iron *K*-edge in pyrite (FeS_2) by using the angular moment method developed for X-ray Natural Circular Dichoism (XNCD) measurements. The natural linear dichroism (XNLD) was found to be around 0.5 % of the edge jump. Experimental results are compared with monelectronic and multilectronic calculations. Calculations allow to quantitatively determine the proportion of quadrupolar transitions in the pre-edge structure and the anisotropy is explained in terms of structural and electronic parameters.

keywords : Electric quadrupole transitions, pyrite

1. Introduction

Electric quadrupole transitions in X-ray absorption spectra have become quite important in the past few years because of their large contribution to X-ray Magnetic Circular Dichroism (Carra *et al.*, 1993). More recently X-ray Natural Circular Dichroism has been measured in various gyrotropic crystals and has revealed interferences between electric dipole and quadrupole transitions (Goulon *et al.*, 2000, and references therein). In this paper, we investigate experimentically and theoretically an effect which is due to purely quadrupole transitions : the angular dependence of X-ray absorption in a cubic crystal.

Electric quadrupole transitions are simpler to measure in cubic crystals, because the electric dipole transitions are isotropic. However the expected quadrupole dependence was not found for neither *bcc*-Fe, nor pyrite (Dräger *et al.*, 1988). More recently the situation changed and a quite strong anisotropy (2 %) was detected in single crystals of NiO and FeO (Heumann *et al.*, 1997), by still measuring the absorption in transmission mode at two angles.

For this study, we chose the case of pyrite for several reasons. Pyrite crystallises in the cubic system, space group $Pa\bar{3}(T_h^6)$. Iron sits in a slightly distorted octahedron of sulphur atoms (point group C_{3i}). In pyrite, iron is divalent and in low-spin states. Thus the t_{2g} orbitals of the metal are completely filled. Consequently, in pyrite the quadrupole transitions involved at the iron *K*-edge are expected to be $1s \rightarrow 3d\text{-}e_g$. From a theoretical point of view, because of the strong covalence of iron with sulphur, we expect that the iron 3*d* orbitals are not too strongly localized and that a one-electron model can work successfully and better than in transition metals oxides.

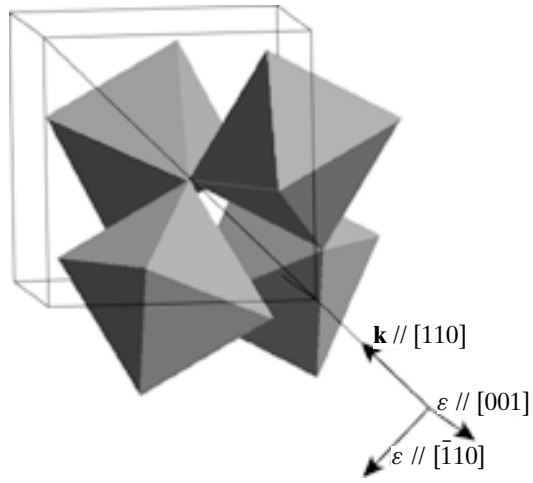

Figure 1
Crystal structure of pyrite. Iron atoms are in C_{3i} site of multiplicity 4, octahedrally coordinated to sulphur atoms. The octahedra are tilted from the crystallographic axis by about 23°. The orientation of the wave vector **k** and the two orientations of the polarisation vector $\boldsymbol{\epsilon}$, leading to maximum dichroic signal, are represented.

2. Experiment and data analysis

According to group theory, for a cubic crystal, the angular dependence of the X-ray absorption can be written as:

$$\sigma(\hat{\boldsymbol{\epsilon}}, \hat{\mathbf{k}}) = \sigma_0 + (\epsilon_x^2 k_x^2 + \epsilon_y^2 k_y^2 + \epsilon_z^2 k_z^2 - \frac{1}{5})\sigma_1,$$

where σ_0 is the isotropic cross section and σ_1 is a purely quadrupolar transition. $\hat{\boldsymbol{\epsilon}}$ and $\hat{\mathbf{k}}$ are the X-ray polarisation and wave unit vectors respectively. As was noticed by Dräger *et al.* (1988), the maximum variation may be obtained by turning the crystal around the [110] direction alined with **k** and by subtracting the absorption obtained with $\boldsymbol{\epsilon}$//[001] from the one obtained with $\boldsymbol{\epsilon}$//[$\bar{1}$10]. The crystal structure of pyrite and the orientation of the single crystal in the X-ray beam are illustrated in Fig. 1.

The experimental data were collected at the ESRF beam line ID12-A, dedicated to polarisation dependent spectroscopies (Goulon *et al.*, 1998). The absorption is measured by eight photodiode fluorescence detectors symmetrically set around the X-ray wave vector. A natural single crystal of pyrite, from Minas Victoria, Logroño (Spain) was oriented, then placed on a rotating holder and turned around the [110] direction, parallel to the X-ray beam direction. Angle 0 corresponds to $\boldsymbol{\epsilon}$//[$\bar{1}$10]. The measurements were not carried out at two angles but, at each energy, the fluorescence intensity was measured by the eight detectors, for 121 angles from 0 to 360°, by step of 3°.

For experiments carried out at the *K*-edge of transition metals in single crystals, it is necessary to be careful with the artefacts coming from the presence of diffraction peaks. Fig. 2 shows the intensity recorded by the eight fluorescence detectors for 120 angles at a fixed energy. The diffraction peaks can come from a diffracted ray that strikes a fluorescence detector or from diffraction that occurs inside the crystal. The presence of diffraction peaks may have a devastating effect on the measurements of absorption spectra. The fact that the data were collected at many angles makes possible to get rid of these artefacts and to use a filtering algorithm based on the angular momentum method developed by Goulon *et al.* (1999)

to measure X-Ray Natural Circular Dichroism. The angular dependence of the intensity recorded by each detector is fitted as a sinusoidal function of the general form:

$$f(\theta) = a + b\cos\theta + c\sin\theta + d\cos 2\theta + e\sin 2\theta, \qquad (1)$$

where θ is the rotation angle. In Eq. 1 a represents the isotropic part of the signal, the dependence on $\cos\theta$ and $\sin\theta$ describes the fact that the rotation axis could be not perfectly alined with the X-ray beam and the fact that the sample could be not perfectly homogeneous, and the dependence on $\cos 2\theta$ and $\sin 2\theta$ should describe the angular dependence. The filtering algorithm operates as follows. A naive fit to the data is carried out, giving a root mean square error σ. Then, each point in turn is selected from the experimental data and a fit is obtained skipping point i. For each of these fits a root mean square error σ_i is calculated. The experimental point causing the largest error is determined by choosing i_0 such that σ_{i0} is the smallest among the σ_i. Then the ratio $\frac{\sigma_{i0}}{\sigma}$ is calculated. If the ratio is greater than 0.95, then the data were considered correct. If the ratio is smaller than 0.95, then point i_0 is removed from the experimental data, and the process is started again. Once the filtering procedure is finished, the parameters of all detectors are summed over.

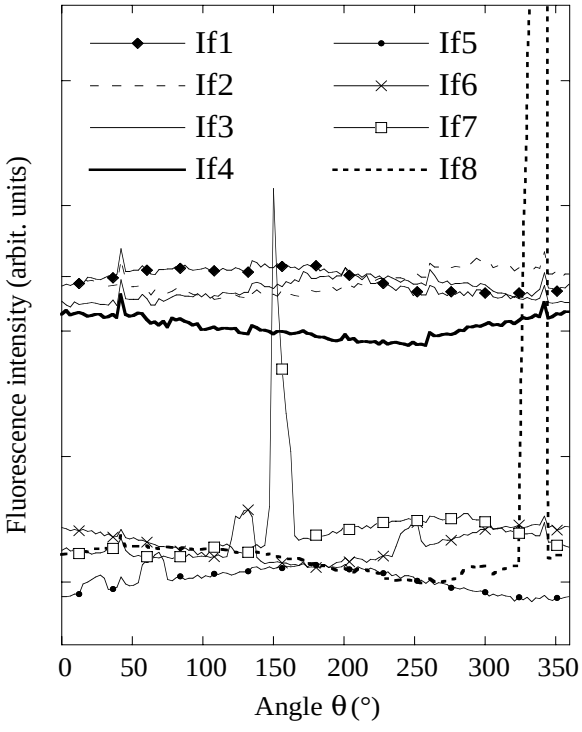

Figure 2
Intensity of the fluorescence signal measyred by eight detectors for a single energy at the iron K-edge in pyrite. The signal is given as a function of the sample holder rotation angle θ.

In our experimental data, the number of points suppressed by the filtering algorithm was most of the time between 0 and 10, with a maximum of 15. The fit coefficients are displayed as a function of energy in Fig. 3. If the sample was perfectly homogeneous and oriented towards the X-ray beam direction, the coefficients b and c should be zero. Fig. 3 shows that through the addition of the signal received by all the fluorescence detectors, the intensity of the $\sin\theta$ and $\cos\theta$ components is strongly decreased, especially below 7120 eV. In other words the eight detectors average out this dependence. It should be noticed that such a result could not be obtained with multiple detectors not symmetrically set around the X-ray beam. Concerning the quadrupole angular dependence, Fig. 3 shows the coefficient e of $\sin 2\theta$ is quite small. This is consistent with the orientation of the single crystal such that [110] direction is along the X-ray beam and [110] corresponds to $\theta = 0$. Consequently the XNLD signal is given by coefficient d of Eq.1. It consists in a single positive peak located in the pre-edge region and its intensity represents about 0.5 % of the edge jump (the XNLD and the XANES are both plotted in Fig. 4).

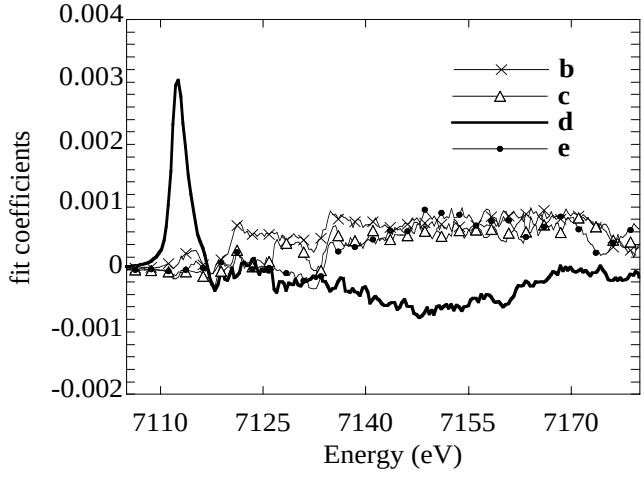

Figure 3
Energy dependence of the fit coefficients. The anisotropy of the Fe K-edge in pyrite is given by d.

3. Calculations

The calculation of the Fe K-XANES and XNLD in pyrite was performed by using the real space non muffin-tin approach of the FDMNES program (Joly *et al.*, 1999). This code calculates the X-ray absorption cross section both in the electric dipolar and quadrupolar approximation by using the Finite Difference Method (FDM) to calculate the monoelectronic wave function in the final state. The main advantage of this technique is that it does not require any approximation on the shape of the potential, so the usual muffin-tin approximation is avoided. In this study, the potential was constructed as follows. Within a 51 atom cluster (i.e. $r = 5.3$Å), a simple superposition of neutral atomic electronic densities was made and the Poisson equation was then solved. To the Coulomb potential so obtained, was added an exchange and correlation potential of Hedin-Lundqvist type. The Z+1 approximation is used to simulate the core-hole and screening effects.

Both experimental (dashed line) and calculated (solid line) spectra are displayed in Fig. 4. A good agreement is obtained for the XANES. The XNLD although small is also correctly reproduced. Since the FDM calculations allow to reproduce the anisotropy, it is then possible to determine the isotropic part of the electric quadrupole transitions. The total cross section, as shown in Fig. 4, is the sum of the electric dipole cross section and the electric quadrupole cross section, and both curves are plotted in the inset of Fig. 4, which a zoom to the pre-edge region is represented. The

isotropic electric quadrupole cross section is about 4 % of the pre-edge intensity and 0.7 % of the edge jump. The pre-edge mainly results from electric dipole transitions.

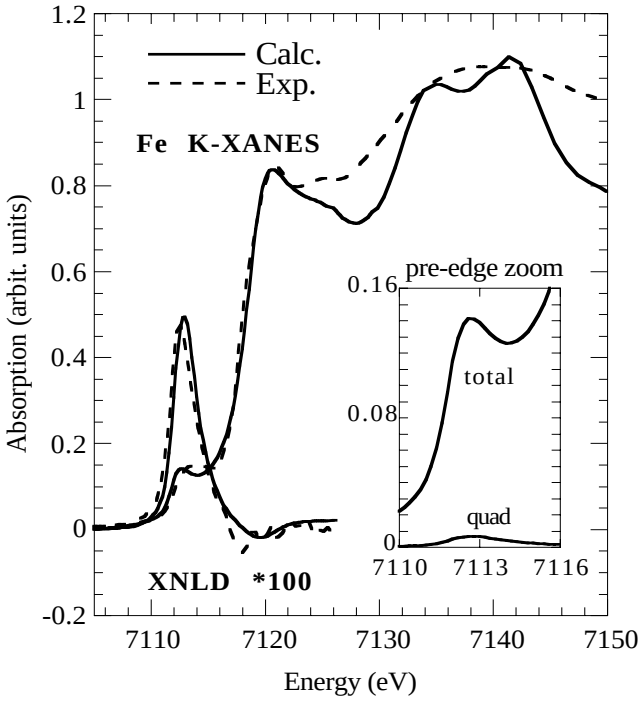

Figure 4
Comparison between experimental (dashed line) and calculated (solid line) Fe *K*-edge spectra in pyrite. The dichroic signal (XNLD) is multiplied by a factor 100. Inset: zoom of the pre-edge region. Both total and electric quadrupole cross sections are plotted.

Density of states calculations were also performed. The FLAPW method of the `Wien97` code was used (Schwarz *et al.*) and a total agreement was obtained with the results of Eyert *et al.* (1998). These calculations have shown that the pre-edge region is majoritary composed of iron 3*d* orbitals. Since the electric dipole operator mainly governs the electronic transitions involved in the pre-edge region, the pre-edge reflects the medium range order through the interaction between the 4*p* orbitals of the absorbing atom and the 3*d* of the iron second neighbours. Because of the centrosymmetry of iron site, the local *p*-*d* hybridization is indeed not possible.

In order to get more insight into the origin of the dichroic signal we have also performed Ligand Field Multiplet calculations in the framework developed by Theo Thole. One has to compute the transitions from the initial state $1s^2 3d^6$ towards the final state $1s^1 3d^7$ for the two experimental set up where $(\boldsymbol{\epsilon}.\mathbf{r}).(\mathbf{k}.\mathbf{r})$ is either equal to $\frac{1}{2}(x^2 - y^2)$ or $\frac{1}{\sqrt{2}}(xz + yz)$. The calculation is first performed for a low spin divalent iron in an undistorted octahedron with the fourfold axis parallel to the z axis of the crystal. For such geometry, one finds that the electric quadrupole dichroic signal is 5/2 times larger than the electric quadrupole isotropic signal. From the simple energy scheme where all the iron t_{2g} orbitals are full and the e_g are empty the dichroism come from allowed transitions when $(\boldsymbol{\epsilon}.\mathbf{r}).(\mathbf{k}.\mathbf{r}) = \frac{1}{2}(x^2 - y^2)$ (e_g symmetry) and forbidden transitions when $(\boldsymbol{\epsilon}.\mathbf{r}).(\mathbf{k}.\mathbf{r}) = \frac{1}{\sqrt{2}}(xz + yz)$ (t_{2g} symmetry). In order to stick to the experiment, one needs to take into account the orientation of the octahedron in the crystal as well as the multiplicity of the iron sites in the unit cell. When this is done, one finds that for an octahedron with a tilt angle of 23° (angle between the four-fold axis of the octahedron and the *z* axis of the crystal) the dichroism is strongly reduced by a factor of ≈ 3 and the ratio $\sigma_{XNLD}/\sigma_{iso}$ is then equal to 0.8 in good agreement with both the experiment and the monoelectronic calculations.

4. Conclusion

A linear dichroic signal has been measured in pyrite. Through multiplet calculations we have developed a simple model, that allows to separate the different contributions to the dichroic signal. The origin of the effect lies as expected from the fact that iron in the low spin state has fully occupied t_{2g} levels and fully empty e_g levels. The tilt of the iron octahedron respectively to the crystallographic axes of the crystals is responsible for a strong reduction of the dichroic signal. In a monoelectronic calculations, where the electronic structure of low spin iron, the tilt and the distortion of the iron octahedra are naturally included, one finds a nice agreement with experiment for the intensity as well as for the shape of the signal.

Acknowledgements

This paper is dedicated to Jacqueline Petiau. We thank Jean-Claude Boulliard and Pierre Bariand who kindly provided the pyrite sample. We are grateful to Alain Jeanne-Michaud for his help in obtaining Fig. 1. Computing time was partially supplied by the "Institut du Développement et des Ressources en Informatique Scientifique". This is IPGP contribution #1719.

References

Carra, P. Thole, B.T., Altarelli, M. & Wang., X. (1993). *Phys. Rev. Lett.* **70**, 694–697.
Dräger, G., Frahm, R., Materlik, G. & Brümmer, O. (1988). *phys. stat. sol. (b)* **146**, 287–294.
Eyert, V., Höck, K.-H., Fiechter, S. & Tributsch, H. (1998). *Phys. Rev. B* **57**, 6350–6359.
Goulon, J., Goulon-Ginet, Ch., Rogalev, A., Benayoun, G., Brouder, Ch. & Natoli, C.R. (2000). *J. Synchrotron Rad.* **7**, 182–188.
Goulon, J., Goulon-Ginet, Ch., Rogalev, A., Benayoun, G., Malgrange, C. & Brouder, Ch. (1999). *X-Ray Optics Design, Performance, And Applications* (Eds. Khousary, A.M., Srajer, G. & Lang, J.) SPIE Proceedings **3773**, 316–325.
Goulon, J., Rogalev, A., Gauthier C., Goulon-Ginet, Ch., Paste, S., Signorato, R., Neumann, C., Varga, L. & Malgrange, C. (1998). *J. Synchrotron Rad.* **5**, 232–238.
Heumann D., Dräger, G. & Bocharov, S. (1997). *J. Phys. IV France, colloque C2* **7**, 481–483.
Joly, Y., Cabaret, D., Renevier, H. & Natoli, C.R. (1999). *Phys. Rev. Lett.* **82**, 2398–2401.
Schwarz, K., Blaha, P. & Luitz, J. WIEN97: a Full Potential Linearized Augmented Plane Wave Package for Calculating Crystal Properties. Techn. Universität Wien/Autria. ISBN 3-9501031-0-4.